JOURNAL OF SOLID STATE CHEMISTRY 102, 480–491 (1993)

Titanium in MFI-Type Zeolites: A Characterization by XANES, EXAFS, IR, and ^{74,49}Ti and ^{17}O MAS NMR Spectroscopy and H_2O Adsorption

A. LOPEZ,* M. H. TUILIER,† J. L. GUTH,‡ L. DELMOTTE,* AND J. M. POPA§

Laboratoire de Matériaux Minéraux, URA CNRS 428, Ecole Nationale Supérieure de Chimie, 3 rue Alfred Werner, 68093 Mulhouse Cedex, France; †Laboratoire de Physique et de Spectroscopie Electronique, URA, CNRS 1435, Faculté des Sciences et Techniques, 4, rue des Frères, Lumière, 68093 Mulhouse Cedex, France; and §Centre de Recherche Rhône Poulenc, 52, rue de la Haie Coq, 93308 Aubervilliers Cedex, France

Received February 3, 1992; in revised form July 10, 1992; accepted July 15, 1992.

The location and chemical environment of titanium in MFI-type zeolites synthesized in OH^- or in F^- media was determined by XANES, EXAFS, IR, and ^{47,49}Ti and ^{17}O MAS-NMR spectroscopy. Water adsorption and its influence on the coordination of Ti was studied in the calcined zeolites. Titanium is incorporated into the framework by substitution for silicon, but a significant amount of Ti can also be present in the form of extracrystalline or intracrystalline inclusions of TiO_2 depending on the F/Ti ratio in the synthesis mixture. In the absence of water, Ti in the framework is essentially tetrahedrally coordinated; in the presence of water its coordination becomes octahedral.

Introduction

MFI-type zeolites with titanium find application as catalysts in oxidation reactions using hydrogen peroxide (*1*). Such materials can be synthesized by hydrothermal crystallization of gels in alkaline (*2*) or neutral medium (*3*). In the last case, F^- anions play the role of mineralizer in place of OH^- (*4*). But until now the location and chemical environment (nature of the ligands, coordination) of titanium has not been clearly proved and completely described (*1*, *5–7*).

X-ray absorption spectroscopy (XAS), joined to other techniques such as solid-state NMR and optical and I.R. spectroscopy, was able to demonstrate the reality of the incorporation of gallium (*8*), germanium (*9*, *10*), and iron (*11*) in the framework of MFI-type zeolites and to obtain accurate information on the local environments of these elements. The problem of titanium in such structures has recently been studied in XAS experiments (*9*, *12*).

The aim of this paper is to extend the preceding results by the study of zeolites obtained by the two different synthesis methods and to confirm them by using, beside XAS experiments, other characterization methods such as IR and solid-state NMR.

‡ To whom correspondance should be addressed.

0022-4596/93 $5.00

In the past years the Ti *K* edge X-ray absorption spectroscopy (XANES, EXAFS) of Ti has been extensively studied in order to improve our knowledge of glassy (*13–18*) and crystalline (*19*) titanium oxides. The changes in the positions and intensities of XANES features have been related to the variation in the geometry of the Ti coordination polyhedra for several natural crystalline oxides (*20, 21*). In addition, theoretical and experimental works on rutile and anatase (*22*) and on $TiCl_4$ (*23*) lead to a better understanding of the effect of four- or six-fold coordination on Ti K XANES spectrum.

Characterization results of Ti in solid oxides by MAS NMR are rather scarce (*24*). One of the aims of this study was to explore the possibilities of this method applied to zeolites containing titanium.

Results of XAS obtained on hydrated and dehydrated samples show that the coordination of Ti depends on the presence or absence of water. This study was completed by a kinetic evaluation of the adsorption of water and the characterization of adsorbed water by IR spectroscopy and ^{17}O MAS NMR.

Experimental

Synthesis

The samples were obtained by hydrothermal crystallization from a gel containing a source of SiO_2 and TiO_2, the organic template $(C_3H_7)_4N^+$ (TPA^+), and either F^- or OH^- ions (*3, 25*). Reaction mixture compositions, heating conditions, and characteristics of the crystals obtained are reported in Table I. The Silica source was either Aerosil 130 from Degussa (F-0, F-2, F-3, F4, OH-0) or tetraorthosilicate from FLUKA (F-1, OH-1). Titanium could be added in different forms: hydrated TiO_2 freshly precipitated from an alcoholic solution of tetrabutylorthotitanate (ALDRICH) (F-0, F-2), tetraethylorthotitanate (FLUKA) to be mixed with tetraethylorthosilicate (F-1, OH-1), H_2TiF_6,xH_2O obtained by dissolving TiO_2 (ALDRICH) in 40% HF (PROLABO) (F-3, F-4.) The templating agent TPA^+ was introduced as TPABr (F samples) or 20% TPAOH (OH samples), both from FLUKA.

Post-synthesis Treatments of the Samples

After the synthesis, the solid phase was recovered by filtration, washed with hot

TABLE I

SYNTHESIS DATA AND CHARACTERISTICS OF THE SAMPLES

Sample	Reaction mixture composition molar ratios					pH[a]	*T*	*t*	Size of			Symmetry[c]	
	Si	Ti	TPA^+	F^-	H_2O	i–f	(K)	(days)	crystals μm	Ti[b]/u.c.	H_2O/u.c.	AS	CH
F-0	1	0	0.25	0.5	40	7–7	448	7	130 × 30 × 30	0	5.9	O	M
F-1	1	0.2	0.25	0.5	40	7–9	473	7	90 × 35 × 15	1.9	nd	O	M
F-2	1	0.1	0.25	0.5	40	7–7.5	473	7	70 × 23 × 20	1.0	nd	O	M
F-3	1	0.1	0.5	1.5	60	7–7	443	7	80 × 20 × 15	0.8	7.7	O	M
F-4	1	0.5	0.5	2	60	7–7	448	7	25 × 15 × 12	1.6	4.5	O	M
OH-0	1	0	0.25	0	25	13.5–13	428	0.6	1–5	0	14.4	O	M
OH-1	1	0.03	0.5	0	25	14–14	448	10	1–5	1.9	13.5	O	O

[a] i–f: initial–final.

[b] Atoms of titanium per unit cell ($Si_{96-x}Ti_xO_{192}$) measured by colorimetry (Ti–H_2O_2 complex) on sonicated samples.

[c] Symmetry of as-synthesized (AS) and calcined and hydrated (CH) samples: O = orthorhombic, M = monoclinic.

water, and dried. A fraction of each solid thus obtained, called the as-synthesized sample (AS), was heated in air at 823 K for 5 Hr to remove the occluded organic molecules and yield the calcined sample. This calcined sample could be left in the surrounding atmosphere to be hydrated (CH) or heated in dry air at 573 K for 4 hr to obtain the dehydrated form (CD).

Residual K^+ ions, present in TPAOH and therefore in OH samples, wee eliminated by an acid treatment of the calcined samples (H_3PO_4, 0.1 *N*, 333 K, 4 h). The ion-exchanged samples thus obtained were recalcined.

Characterization

X-ray absorption spectroscopy. The X-ray absorption experiments were performed at the LURE-DCI synchrotron radiation source (Orsay, France). The data were collected at room temperature, in transmission mode. Finely powdered samples with a particle size calibrated to less than 20 μm, using a mesh, were put between two kapton windows. In order to study the effect of dehydration, the calcined and dehydrated OH-1(CD) sample was placed in the beam within a tight dry N_2-filled box. Due to the low concentration of titanium in the samples (about 1.5% by weight) and the strong absorption of silicon at the Ti *K* edge, thickness was carefully optimized. The best value of the edge step $\Delta(\mu x)$ was found to be 0.2–0.3. The X-ray beam supplied at the EXAFS 2 station was monochromatized by a Si (311) two-crystal spectrometer. The beamline was equipped with a harmonic rejection device made of two parallel mirrors at 4 mrd.

The data were analyzed using the computer software described in Ref. (*26*). In XANES and EXAFS spectra, the preedge absorption, which presents a very strong slope, was fitted by a Victoreen function. The threshold energy E_0 has been taken at the inflection point of the Ti *K* edge (E_0 = 4979.5 eV) (*27*). The XANES spectra were normalized to the background absorption above the Ti *K* edge (edge height). The energy values of the preedge features given in Tables II and III are taken from the first inflexion point of Ti metal *K* absorption.

The structural information of EXAFS is contained in the oscillatory modulation of the absorption coefficient above the *K* edge, $\chi(k)$. k is the electron wave vector defined as

$$k = [(2m/h^{-2})(E - E_0)]^{1/2},$$

where E is the photon energy, E_0 the threshold energy, and m the mass of the electron, respectively. The complete analysis of $\chi(k)$ yields the interatomic distances between the absorber and its near neighbors, R, the number of these neighbors, N, and the Debye–Waller factor, σ^2, which arises from both structural disorder and thermal motion in a given shell (27).

The continous absorption above the Ti *K* edge was fitted to a polynomial or a spline function. After conversion to k space, the normalized $\chi(k)$ data were multiplied by k^3 and Fourier transformed between 3 and 9 or 11 $Å^{-1}$. The first neighbor's peak in Fourier transforms (FT) was filtered in R space. The structural parameters R, N, and σ^2 were extracted by least-squares refinements. The results given in Table IV were obtained using the experimental phase shifts extracted from the analysis of the model compound TiO_2 rutile. Ba_2TiO_4, where titanium is in fourfold coordination, should be a suitable model compound. Unfortunately the Ba L_{III} absorption occurs about 200 eV above the Ti *K* edge and makes it unusable. The calculations were checked by using Teo (*27*) and McKale *et al.* (28) theoretical phase shifts. The latter takes into account the curve of the electron waves. The fits of Table IV were obtained by minimizing the function

TABLE II

Ti *K* PREEDGE PARAMETERS AND SITE SYMMETRY IN SOME TITANIUM REFERENCE COMPOUNDS

Compound	Ti-coordination	Position (eV)[a]	Intensity[b]	FWHM (eV)[c]	Symmetry of the site
Benitoite		2.6	0.03		Slightly
[20, 21]	6	5.1	0.03	–	distorted octahedron
TiO_2 anatase		2.6	0.07		distorted
(this work)	6	5.4	0.14	–	octahedron
		8.2	0.13		
TiO_2 rutile		2.9	0.03		distorted
(this work)	6	5.6	0.16	–	octahedron
		8.9	0.14		
Biotite					very
[20, 21]	6	4.6	0.27	2.5	distorted octahedron
Kaersutite					very
[20, 21]	6	4.5	0.30	2.5	distorted octahedron
Titanyl phtalocyanine [15]	5	4.5	0.79	1.9	square pyramid
$TiCl_4$					regular
[14, 22]	4	3.5	0.57	2.2	tetrahedron
Ba_2TiO_4	4	3.5	0.85	1.5	distorted tetrahedron

[a] Taken from the first inflexion point of Ti metal *K* absorption spectrum (±0.2 eV).
[b] Related to the edge height (see experimental section).
[c] Full width at half maximum.

$$F = \sum_k W(k) \frac{[k\chi \exp(k) - k\chi \text{ cal}(k)]^2}{\sum_k W(k)[k\chi \exp(k)]^2}$$

with $W(k) = k^3$.

MAS-NMR spectroscopy. Solid state NMR measurements were carried out on a Bruker MSL 300 multinuclear spectrometer.

^{29}Si and ^{17}O MAS NMR spectra were recorded at 59.6 and 40.7 MHz, respectively. The chemical shifts were given in ppm with respect to the external standards: tetramethylsilane (TMS) for ^{29}Si NMR and H_2O for ^{17}O NMR.

^{47}Ti and ^{49}Ti broadband spectra were obtained at 16.9 MHz using a quadrupolar multiecho pulse sequence (*29*).

Water adsorption. Adsorption of water was followed by thermogravimetric analysis on a Setaram TGA92 instrument. Before adsorption, samples were degassed at 573 K under a vacuum of 1 mbar for 1 hr. After cooling to 298 K, the relative pressure of water over samples was adjusted to $P/P_0 = 0.9$.

IR spectra. IR spectra were recorded on a Bruker IFS 66 spectrometer using the KBr pellet technique. These pellets were prepared with 0.25% of well crushed zeolite powder and then exposed to the surrounding atmosphere (hydrated samples) or dried at 373 K for 1 hr (dehydrated samples).

Results

XANES

The main structural information inferred from Ti *K* XANES spectra comes from the shape of the preedge features close to the rising edge, which corresponds to dipole-allowed $1s$–$4p$ transitions. The preedge structure is attributed to $1s$–$3d$ transitions, which are dipole-forbidden in free atoms

TABLE III

CHARACTERISTICS OF THE *K* PREEDGE IN TITANIUM MFI TYPE ZEOLITES

Sample	Position[a] (eV)	Intensity[b]	FWHM[c] (eV)
F-1(AS)	3.0	0.08	
	5.3	0.13	–
	8.5	0.12	
F-2(AS)	2.8 sh	0.10	
	4.6	0.19	–
	5.9 sh	0.13	
	8.6	0.11	
F-3(AS)	4.3	0.26	1.9
F-4(AS)	4.4	0.28	1.9
F-2(CH)	2.8 sh	0.09	
	4.6	0.20	–
	5.9 sh	0.12	
	8.6	0.11	
F-4(CH)	4.1	0.40	1.7
OH-1(CH)	4.5	0.27	2.3
OH-1(CD)	3.8	0.50	1.5
OH-1(CH2)	4.5	0.27	2.3

[a] Taken from the first inflexion point of the Ti metal *K* absorption spectrum (±0.2 eV); sh means shoulder.

[b] Related to the edge height (see experimental section).

[c] Full width at half maximum.

and in environments with inversion centers. Without inversion symmetry, as for example in tetrahedral coordination (T_d), $3d4p$ mixing causes dipole-allowed transition to at least one of the ligand-field-split final states ($1s$ to t_2 in T_d) (22). Moreover, due to the d^0 configuration of Ti^{4+} there is no d–d multiplet structure.

Several compounds supplied references for the interpretation of the Ti *K* XANES in the studied zeolites. Their preedge positions and intensities and the nature of their coordination polyhedron are listed in Table II. For regular octahedral coordination, as for example in benitoite, the preedge intensity is very low. In kaersutite, Ti^{4+} cations fill several distorted sites and single rather high preedge peak is observed. Indeed, bond angle deviations from 90° in octahedra should increase $3d4p$ mixing into the final state of the preedge transition, increasing the absorption probability (*20*, *21*). In rutile and anatase, the preedge is split into several components with lower intensities.

The absence of the inversion centre in penta- and tetracoordinated titanium compounds yields single preedge peaks. The higher preedge intensity in Ba_2TiO_4 as compared to $TiCl_4$ should be related to the shorter bond length between titanium and oxygen, which increases the orbital overlap, and/or to the increase of $3d4p$ mixing in distorted coordination polyhedra (see below).

The Ti *K* XANES spectra of as-synthesized zeolite samples are presented in Fig. 1. The positions and intensities of the pre-

TABLE IV

STRUCTURAL PARAMETERS OF THE FIRST COORDINATION SHELL OF TITANIUM FROM EXAFS ANALYSIS IN CALCINED AND HYDRATED OH-1(CH) AND CALCINED AND DEHYDRATED OH-1(CD) SAMPLES

Sample	N_1[a]	R_1 (Å) ±0.02 Å	$\Delta\sigma_1^{2b}$ $\times 10^3$(Å^2)	N_2[a]	R_2 (Å) ±0.05 Å	$\Delta\sigma_2^{2b}$ $\times 10^3$(Å^2)	F $\times 10^3$
OH-1(CH)	5.9	1.90	7.4	–	–	–	0.7
OH-1(CD)	3.5	1.84	1.6	–	–	–	9
	3.4	1.83	1.6	0.8	1.97	6.4	8

[a] Number of oxygen neighbors in a given shell or subshell around titanium.

[b] Debye–Waller parameter in a given shell or subshell: $\Delta\sigma_i^2 = [\sigma_i^2 - \sigma_{ref}^2]$. Rutile-type TiO_2 was used as reference compound.

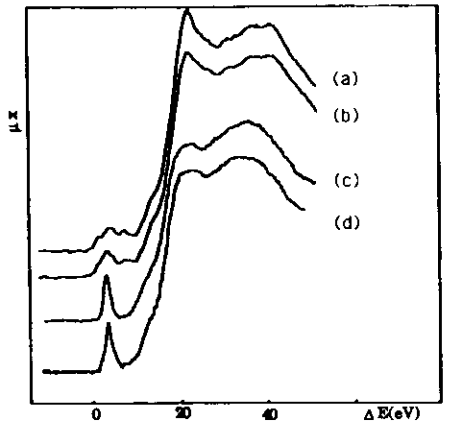

FIG. 1. Ti *K* XANES spectra of as-synthesized zeolites: (a) F-1(AS), (b) F-2(AS), (c) F-3(AS), (d) F-4(AS).

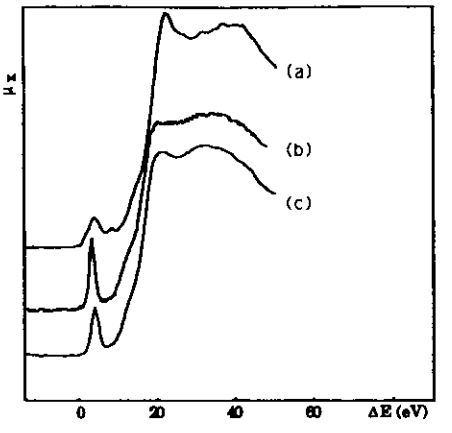

FIG. 2. Ti *K* XANES of calcined and hydrated zeolites. (a) F-2(CH), (b) F-4(CH), (c) OH-1(CH).

edge features are reported in Table III. The preedge of the as-synthesized F-1(AS) is similar to that of anatase.

The F-3(AS) and F-4(AS) give broad preedge peaks which suggest octahedral environments like those in kaersutite (Tables II and III). Nevertheless a fivefold coordination must also be considered. The shape of the F-3(AS) and F-4(AS) spectra probably results from several distorted environments. F-2(AS) presents intermediate behavior which suggests that a part of the titanium is in TiO_2 form and another part is as in F-3(AS) and F-4(AS).

The effect of the calcination and rehydration on F-2(AS) and F-4(AS) was studied (Fig. 2 and Table III). In the calcined and rehydrated F-4(CH), the preedge peak becomes sharper and narrower and it is slightly shifted toward the lower energies. This behavior suggests that at least some Ti sites evolve toward tetrahedral coordination and rules out a strong contribution of TiO_2 as in F-1(AS). In contrast, the calcination has no effect on F-2(AS) (Fig. 2 and Table III) and the major part of titanium is probably under the TiO_2 form.

Titanium keeps its octahedral symmetry in calcined and rehydrated sample OH-1(CH) (Fig. 2). However, in calcined and dehydrated sample OH-1(CD), the preedge peak changes strongly and becomes closer to that observed in fourfold coordination (Ba_2TiO_4) (Fig. 3 and Tables II and III). After rehydration of OH-1(CD), the spectrum of OH-1(CH2) recovers the same aspect as in OH-1(CH), which shows the reversibility of the hydration–dehydration effect.

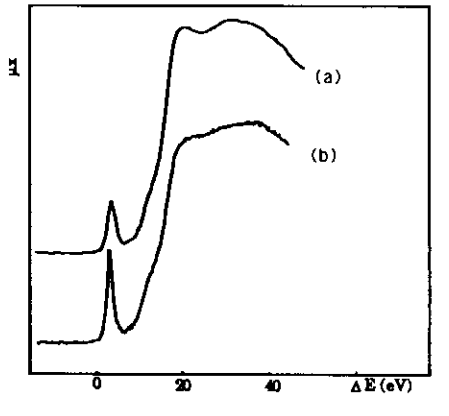

FIG. 3. Ti *K* XANES of (a) rehydrated sample OH-1(CH) and (b) dehydrated sample OH-1(CD).

EXAFS

The OH-1 sample is well suited to evidence the incorporation of titanium in the zeolite framework. From XANES, the titanium environment is revealed to be clearly octahedral in the calcined and hydrated sample OH-1(CH), whereas in the calcined and hydrated samples F-3(CH) and F-4(CH), titanium probably occupies various sites. Furthermore, titanium evolves reversibly toward fourfold coordination after dehydration in sample OH-1(CH).

The $k\chi(k)$ data of OH-1(CH) and OH-1(CD) samples and rutile-type TiO_2 are presented in Fig. 4. In the Fourier transforms of $k^3\,\chi(k)$ data (Fig. 5), significant differences are observed between the two zeolite samples. The peak below 1 Å is due to the residual noise arising from the strong absorption of silicon and oxygen contained in the zeolite network and has no physical meaning. The peak around 1.5–2 Å, which corresponds to the first oxygen neighbors around titanium, appears at a shorter distance in the dehydrated OH-1(CD) sample than in the hydrated OH-1(CH) one.

The results of the refinements (Table IV) and Fig. 6 confirm the XANES observations and the evolution in the FT. In the hydrated OH-1(CH) sample, the number of neighbors is close to 6 and the Ti–O distance is 1.90 Å, which is an acceptable value for sixfold coordination (Fig. 6a). After dehydration of OH-1(CD), the Ti–O distance drops to 1.83 Å and the number of neighbors decreases, whereas the lower value of σ^2 indicates an increase of the local order around titanium. Nevertheless, the quality of the refinement is slightly improved by introducing into the calculation a second oxygen subshell at a higher distance (1.97 Å). The results of the two-shell fit (Fig. 6b) agree with a mixing of 85% of tetrahedral sites and 15% of octahedral sites.

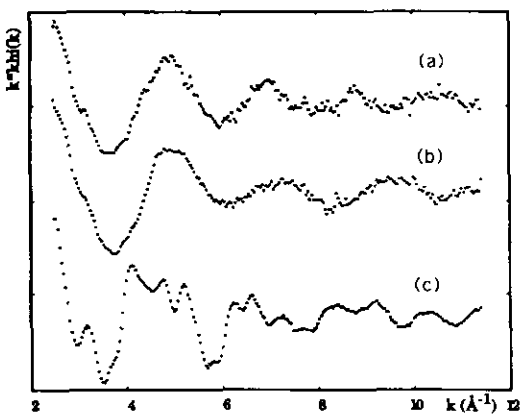

FIG. 4. EXAFS data of (a) rehydrated sample OH-1(CH), (b) dehydrated sample OH-1(CD), and (c) rutile-type TiO_2.

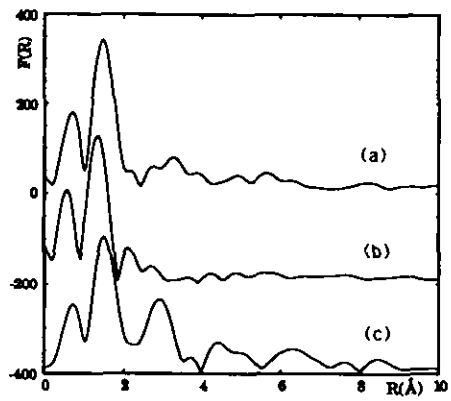

FIG. 5. Fourier transforms of $k^3\,\chi(k)$ data of (a) rehydrated sample OH-1(CH), (b) dehydrated sample OH-1(CD), and (c) rutile-type TiO_2. ($F(R)$ in arbitrary units.)

^{29}Si and $^{47\text{-}49}Ti$ MAS NMR

^{29}Si MAS NMR spectra of as-synthesized samples and calcined samples prepared in fluorine media show a loss of resolution in comparison with the titanium-free samples (Fig. 7). That expresses an increase in the number of different environments for every initial Si site which can be explained by the substitution of Ti and Si in the framework and/or the creation of defaults (unoccupied sites, nonbridging). The shoulder between −114 and −177 ppm reported by Perego

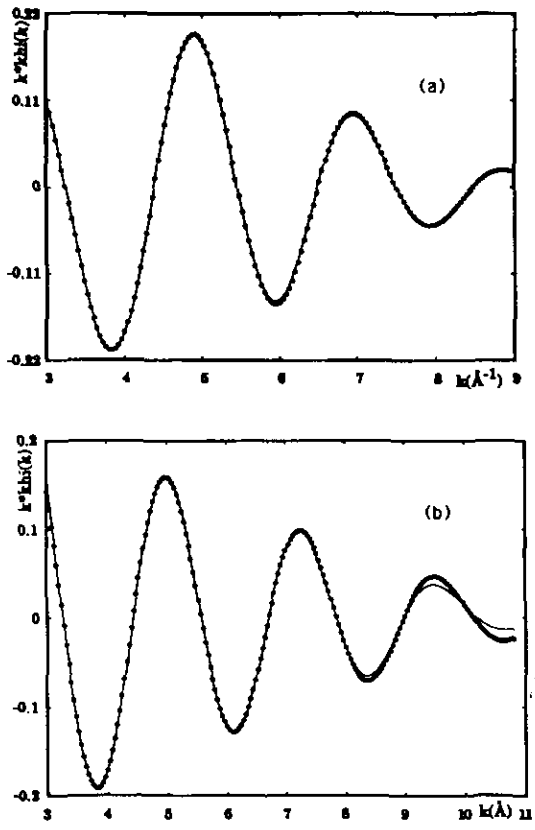

FIG. 6. Oxygen contributions to the EXAFS signal: experimental data (dots) and calculated curves with the parameters of Table IV (solid lines) for (a) hydrated sample OH-1(CH) and (b) dehydrated sample OH-1(CD) (model with two subshells of oxygen neighbor).

et al. (*30*) and present on the spectrum of our OH-1(CH) sample can be related to the orthorhombic symmetry of such samples (*31*) and is not closely connected to the incorporation of Ti in the tetrahedral sites of the framework. The absence of this shoulder on the spectra of sample F-3 is due to the symmetry of these samples which remains monoclinic even when a large amount of titanium is incorporated.

Because of the technical difficulties associated with the analysis of the $^{47-49}$Ti nuclei in the solid state (low frequency, ringing effect, strong quadrupolar interaction), no study was published until then. Only $BaTiO_3$ gives a sharp signal owing to the perfect octahedral environment of Ti (cubic symmetry at 393 K) (*24*). Thanks to the use of an antiringing pulse sequence, (*29*), some $^{47-49}$Ti signals were obtained with our titanium MFI-type zeolite samples. Figure 8 shows the $^{47-49}$Ti spectra of OH-1(CH) and OH-1(CD) samples in comparison with TiO_2 rutile and Ba_2TiO_4 references spectra. The slight distortion of the octahedron in TiO_2 rutile induces a strong broadening of the signal (~100,000 Hz compared to ~2000 Hz in $BaTiO_3$). For Ba_2TiO_4, because of the drastic fall in symmetry (lack of inversion center and distortion of the Ti site), the signal overlies the entire spectral width.

The disappearance of the signal after dehydration of the OH-1(CH) sample can be understood by analogy with the spectra of the Ba_2TiO_4 reference compound. So the

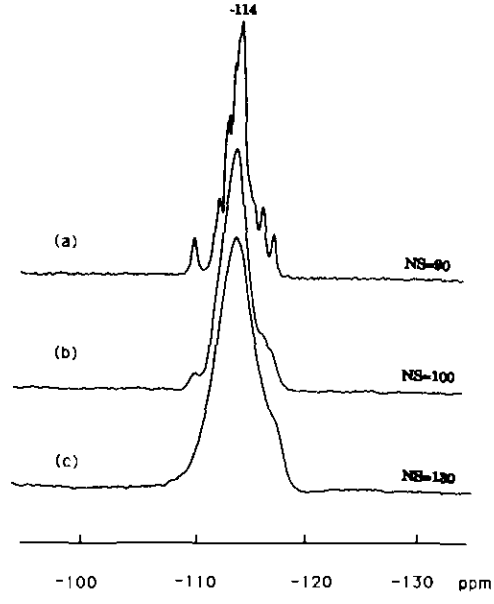

FIG. 7. ^{29}Si MAS NMR spectra of calcined and hydrated samples: (a) F-0(CH), (b) F-2(CH), and (c) F-4(CH). (NS = number of scans.)

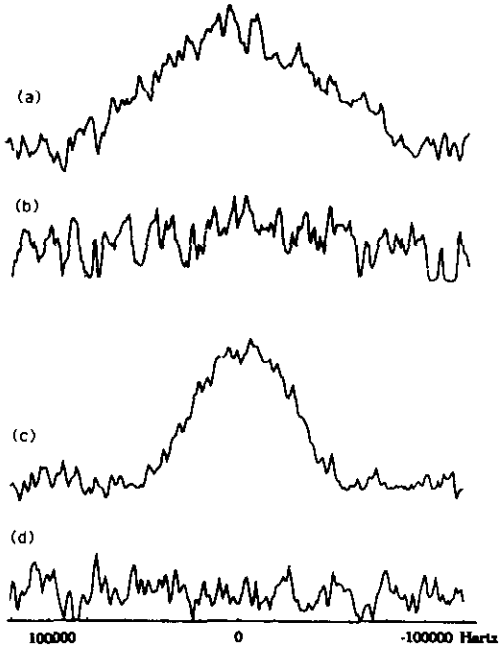

FIG. 8. $^{47-49}$Ti MAS NMR of (a) TiO_2 rutile (coordination of Ti: 6), (b) Ba_2TiO_4 (coordination of Ti: 4), (c) sample OH-1(CH), and (d) sample OH-1(CD).

environment of Ti seems to be close to octahedral coordination in the OH-1(CH) sample and to tetrahedral coordination in the OH-1(CD) sample.

As X-ray absorption and NMR spectra show pronounced differences between hydrated and dehydrated samples, it was of interest to study the adsorption of the water.

Water: Adsorption properties, ^{17}O MAS NMR, and infrared spectroscopy

Figure 9 illustrates the adsorption and desorption of H_2O for the F-0(C) and F-1(C) samples (OH samples present the same behavior). The difference between the two shapes, i.e., F-1 shows a more rapid adsorption and a lower desorption rate, indicates a stronger interaction with H_2O for the sample containing titanium. We note that there is no correlation between the total quantity of adsorbed H_2O and the amount of titanium incorporated (see Table I). That can be explained by the very small quantities of H_2O involved which are probably affected by variations in the number of silanol groups (hydrophilic sites).

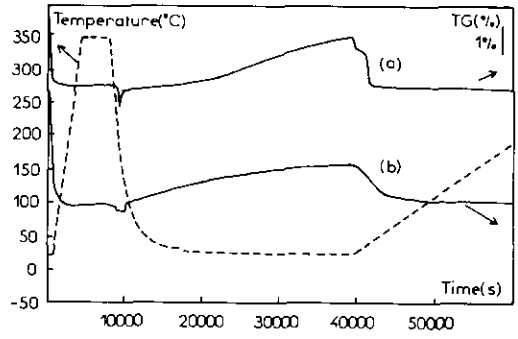

FIG. 9. Hydration and dehydration evolution of samples (a) F-0(C) and (b) F-4(C) as a function of the temperature and time (P/P_0 of water vapor ~0.85).

The study of hydrated samples by ^{17}O MAS NMR confirmed the presence of a specific interaction between Ti sites and H_2O molecules. Indeed Fig. 10 shows an intense and sharps ^{17}O signal for the sample containing titanium, OH-1(CH), and a broad signal characteristic of nonspecific interactions of $H_2{}^{17}O$ with the framework in the sample not containing titanium, OH-0(CH).

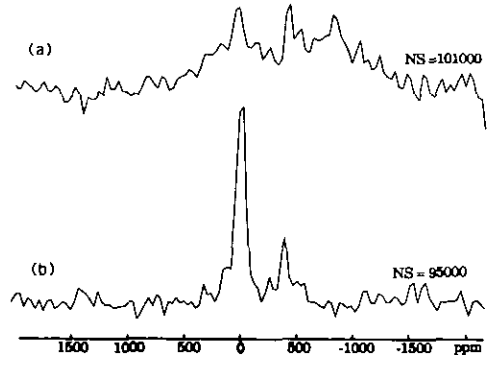

FIG. 10. ^{17}O MAS NMR spectra of samples (a) OH-0(CH) and (b) OH-1(CH). (NS = number of scans.)

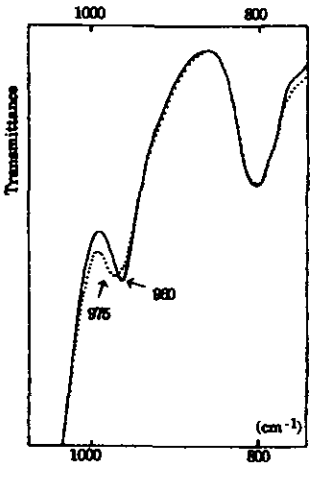

FIG. 11. Influence of the hydration on the position of the infrared absorption peak corresponding to the vibration of the SiO_4 tetrahedra linked to Ti: (a) ··· F-4(CH), (b)—F-4(CD).

The effect of the adsorption of H_2O in titanium MFI-type zeolites can also be observed by infrared spectroscopy. Figure 11 compares the shape and the position of the band near 970 cm before and after hydratation of the F-4(C) sample. The observed modifications were reported by Boccuti *et al.* (32).

Discussion and Conclusion

The similarity between the XANES spectra of F-1(AS) and anatase or rutile clearly confirms the presence of condensed titanium oxides in that sample. They form nanosized inclusions in the MFI-type crystals as previously shown by scanning electron microscopy, X-ray emission mapping, and electron nanoprobe analysis (*25*). The percentage of Ti in the form of such inclusions, estimated from the XANES spectra by comparison with spectra of samples containing known amounts of TiO_2, decreases from 90% to 100% (F-1(AS)) to 30%–40% (F-2(AS)) and 0%–10% (F-3(AS) and F-4(AS)). In the case of large amounts of intra- or extracrystalline TiO_2, the presence of eventual framework titanium can only be evidence by infrared spectroscopy (see below). The examination of the XANES spectra of the calcined samples leads to the same conclusion about condensed TiO_2.

The nature of Ti, other than in TiO_2, was essentially studied in the two samples F-4 and OH-1 which do not contain such oxides. The intensity and position of the pre-edge peak on the XANES spectra of the calcined and hydrated samples are in agreement with "diluted" Ti atoms in an oxide structure with octahedral coordination, as in such reference samples as biotite or kaersutite. The weak shift and the higher intensity observed in the spectrum of F-4(CH) can be explained by the presence of some titanium with tetrahedral coordination (estimated to be about 30%–40% of the total Ti). But it can be noted that the corresponding as-synthesized sample probably contains only Ti with octahedral coordination.

These preliminary results are completed by the EXAFS study on the two OH-1(CH) and OH-1(CD) samples which shows in addition that a reversible change in the coordination degree occurs during dehydration (from ~100% octahedral to a mixture of ~15% octahedral and ~85% tetrahedral). Thus we can assume the existence of an *equilibrium between anhydrous fourfold* coordinated titanium (I) and two sixfold coordinated titanium (II and III):

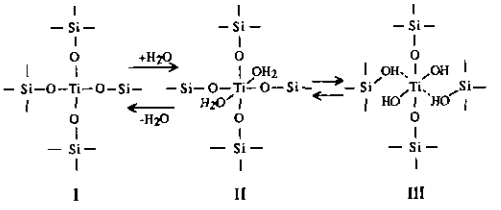

According to the EXAFS study results, structure (III) seems to be more likely in the presence of water. Indeed, if the four Ti–O–Si bonds were intact with a Ti–O distance of 1.83 Å, then the two oxygens of the

water molecules in (II) should be at a distance of more than 2.0 Å from Ti in order to yield the observed mean distance of 1.90 Å. In this case the difference between the shortest and longest bounds would lead to a high σ in the EXAFS analysis, requiring a two shell fitting for the hydrated sample.

The structure (III) is also consistent with the infrared absorption band observed near 970 cm^{-1}. This band was first assigned to Ti=O groups (*1*). But Boccuti *et al.* (*32*) excluded this hypothesis on the basis of their results on titanosilicalites which can be explained by the presence of Si–OH groups and Ti–O–Si bonds. It must be borne in mind that silanol groups are always present in MFI-type crystals: even in the absence of Ti there is a shoulder between 950 and 970 cm^{-1}. But two facts must be noted: in the presence of Ti there is an increase in the intensity of the band with the amount of Ti, and a shift occurs during hydration toward higher wavenumber, with broadening of the band. Thus we assume that the absorption at 960 cm^{-1} is essentially due to the increased degeneracy of the elongation vibration in the framework SiO_4 tetrahedra induced by the change in the polarity of the Ti–O bond when Si is linked to Ti. The SiOH groups formed by the hydrolysis of the Ti–O–Si bonds and sharing OH with Ti (cf. Structure III) are then responsible for the absorption at higher wave numbers (*32*) compared to the values for normal Si–OH groups (*33*).

The linewidth broadening observed on the ^{29}Si MAS NMR spectra in the presence of Ti can only be used as an indication of a possible incorporation of Ti in the framework because other factors (e.g., presence of defects, distortion of the framework due to species in the channels) could also, be responsible for this observation. On the other hand the results of the $^{47-49}Ti$ MAS NMR experiments constitute a better proof. They confirm furthermore the change of coordination during hydration.

Finally, the strong specific interaction between water and the Ti sites, with the formation of hydroxyl ligands, is clearly shown by the narrow peak observed on the ^{17}O MAS NMR spectrum obtained after adsorption of ^{17}O MAS NMR labeled water. The high affinity of water for the Ti sites also significantly influences its adsorption and desorption rates.

In conclusion, a model could be proposed from analysis of the XANES and EFAFS spectra accounting for the role of titanium (localization and chemical environment) in hydration of MFI-type crystals. In the absence of water titanium substitutes for silicon in the framework with tetrahedral coordination. In the presence of water two of the Ti–O–Si bridges hydrolyse to form octahedrally coordinated titanium.

This interpretation is comforted by the results obtained with several other techniques (NMR, IR).

The results of this study also show that, according to the synthesis method and reaction mixture composition, different types of titanium may be present and the hydration of the Ti sites in the framework may be more or less complete. All these observations are important if such solids are to be used as oxygenation catalysts with H_2O_2, which probably has the same behavior as water.

References

1. B. NOTARI, *in* "Studies in Surface Science and Catalysis" (P. J. Grobet, W. J. Martin, E. F. Vansant, and G. Schultz-Ekloff, Eds.) Vol. 37, p. 413, Elsevier, Amsterdam (1988).
2. M. TARAMASSO, G. PEREGO, AND B. NOTARI, US Pat. 4,410,501 (1983)
3. J. L. GUTH, H. KESSLER, AND J. M. POPA, French Pat. Appl. 87/07187 (1987).
4. J. L. GUTH, H. KESSLER, J. M. HIGEL, J. M. LAMBLIN, J. PATARIN, A. SEIVE, J. M. CHEZEAU, AND R. WEY, *in* "Zeolite Synthesis" (M. L. Occelli and H. E. Robison, Eds.) ACS Symposium

Series, Vol. 398, Am. Chem. Soc., Washington, (1989).
5. B. KRAUSHAAR-CZARNETZEI AND J. H. C. VAN HOFF, *Catal. Lett.* **2,** 43 (1989).
6. T. TATSUMI, M. NAKAMURA, S. NEGISHI, AND H. TOMINAGA, *J. Chem. Soc. Chem. Commun,* 476 (1990).
7. D. R. C. HUYBRECHTS, L. DE BRUYCKER, AND P. A. JACOBS, *Nature* **345,** 240 (1990).
8. S. A. AXON, K. HUDDERSMAN, AND J. KLINOWSKI, *Chem. Phys. Lett.* **172,** 398 (1990).
9. A. LOPEZ, M. H. TUILIER, H. KESSLER, J. L. GUTH, AND J. M. POPA, "X-Ray Absorption Fine Structure" (S. S. Hasnain, Ed.), p. 549, Ellis Herwood, New York (1991).
10. M. H. TUILER, A. LOPEZ, J. L. GUTH, AND H. KESSLER, *Zeolites* **11** (7), 662 (1991).
11. J. PATARIN, M. H. TUILIER, J. DÜRR, AND H. KESSLER, *Zeolites* **12** (1), 70 (1991).
12. P. BEHRENS, J. FELSCHE, AND W. NIEMANN, *Catal. Today* **8,** 479 (1991).
13. D. R. SANDSTROM, F. W. LYTLE, P. S. P. WEI, R. B. GREEGOR, J. WONG, AND P. SCHULTZ, *J. Non-Cryst. Solids* **41,** 201 (1980).
14. R. B. GREEGOR, F. W. LYTLE, D. R. SANDSTROM, J. WONG, AND P. SCHULTZ, *J. Non-Cryst. Solids* **55,** 27 (1983).
15. C. A. YARKER, P. A. V. JOHNSON, A. C. WRIGHT, J. WONG, R. B. GREEGOR, F. W. LYTLE, AND R. M. SINCLAIR, *J. Non-Cryst. Solids* **79,** 117 (1986).
16. M. EMILI, L. INCOCCIA, S. MOBILIO, G. FAGHERAZZI, AND M. GUGLIELMI, *J. Non-Cryst. Solids* **74,** 129 (1985).
17. T. DUMAS AND J. PETIAU, *J. Non-Cryst. Solids* **81,** 201 (1986).
18. B. POUMELLEC, B. MARUCCO, AND B. TOUZELIN, *Phys. Rev.* **B 35,** 2284 (1987).
19. F. BABONNEAU, S. DOEUFF, A. LEUASTIC, C. SANCHEZ, C. CARTIER, AND M. VERDAGUER, *Inorg. Chem.* **27,** 3166 (1988).
20. G. A. WAYCHUNAS, *J. Phys. C8* **47,** 841 (1986).
21. G. A. WAYCHUNAS, *Am. Mineralogist* **72,** 89 (1987).
22. V. KUETGENS AND J. HORMES, *in* "2nd Conf. on Progress in X-Ray Synchrotron Radiation Research" (A. Balerna, E. Bernieri, and S. Mobilio, Eds.) Conf. Proc. Vol. 25, p. 59, SIF, Bologna (1990).
23. R. BRYDSON, H. SAUER, W. ENGEL, J. M. THOMAS, E. ZEITLER, N. KOSUGI, AND H. KURODA. *J. Phys. Cond. Matter* **1,** 797 (1989).
24. A. FORBES, "NMR Spectra from the Application Laboratory of Bruker," p. 12, Bruker, Karlsruhe (1986).
25. A. LOPEZ, Thesis Unversity of Haute-Alsace (1990).
26. A. MICHALOVICZ, "Logiciels pour la Chimie," p. 102, SFC, Paris (1991).
27. B. K. TEO, "EXAFS: Basic Pinciples and Data Analysis," Springer-Verlag, Berlin (1986).
28. A. G. MCKALE, B. W. VEAL, A. P. PAULIKAS, S. K. CHAN, AND G. S. KNAPP, *J. Am. Chem. Soc.* **110,** 3763 (1988).
29. A. C. KUNWAR, G. L. TURNER, AND E. OLDFIELD, *J. Magn. Reson.* **69,** 124 (1986).
30. G. PEREGO, G. BELLUSSI, C. CORNO, M. TARAMASO, F. BUONOMO, AND A. ESPOSITO, "New Developments in Zeolite Science and Technology" Vol. 28, (Y. MURAKAMI, A. IIJIMA AND J. W. WARD, EDS.), Studies in Surface Science and Catalysis, p. 129, Elsevier, Amsterdam (1986).
31. G. DEBRAS, A. COURGUE, J. NAGY, AND DE G. CLIPPELEIR, *Zeolites* **6**(3), 161 (1986).
32. M. R. BOCCUTI, K. M. RAO, A. ZECCHINA, G. LEOFANTI, AND G. PETRINI, "Structure and Reactivity of Surfaces" (G. Morterra, A. Zecchinia, and G. Coste, Eds.), p. 133, Elsevier, Amsterdam (1989).
33. D. L. WOOD AND E. M. RABINOVICH, *Appl. Spectrosc.* **43**(2), 263 (1989).